Computer Simulation for Surfactant Vesicle Photopolymerization

Wayne F. Reed*

Department of Physics, Clarkson University, Potsdam, New York 13676.
Received January 21, 1985

ABSTRACT: Based on a recently developed experimental model for photoinitiated surfactant vesicle polymerization, a simulation program has been written to analyze the polymerized vesicles' surface morphology and to calculate the distributions of the polymer fragment chain lengths. The simulation substantiates the experimental evidence that clefts or pockets are formed on the polymerized vesicle surface due to the contraction of monomer headgroup separations caused by the polymeric bonding and gives distributions and values for the cleft sizes and other parameters. Several simulations are also carried out on vesicles composed of polymerizable monomers that would yield different polymeric bond lengths and/or different average chain lengths.

Introduction

Bilayer vesicles made from synthetic surfactants and those made from naturally occurring amphiphilic molecules (liposomes) find a wide field of application in the study of membrane properties and membrane-mediated processes,[1] the microthermodynamics of small systems and self-organizing molecular assemblies, and other fundamental protobiological and biological phenomena.[2] Areas of practical application include the compartmentalization of reactants for enhancing chemical rates and altering reaction pathways, the in situ generation of catalytic particles and other colloids, and the spatial configuring of light-sensitive and redox compounds for solar energy conversion and other novel photochemical systems.[3]

The increased use of surfactant vesicles in such investigations has led to the development of a large variety of synthetic amphiphiles,[4] which confer different properties on the vesicles prepared from them (e.g., size, surface charge, stability, etc.). In an effort to increase the stability of vesicles and other self-organizing media and to influence their surface characteristics, surfactants have been synthesized[5-9] that contain polymerizable moieties at a selected site on the headgroup or along the hydrocarbon tail. When vesicles are prepared from these surfactants, intravesicular polymerization can be initiated by standard chemical initiators (e.g., AIBN, persulfate, etc.) or by irradiation with ultraviolet light when a suitable chromophore is present in the polymerizable moiety.

Studies of such vesicles have been carried out in this laboratory, and the kinetics and mechanism of the photopolymerization of vesicles prepared from a prototypical quaternary ammonium surfactant containing a styrene moiety off the headgroup ($[n\text{-}C_{15}H_{31}CO_2(CH_2)_2]_2N^+[CH_3][CH_2C_6H_4CH{=}CH_2]Cl^-$) (Figure 1) have been established by using laser spectroscopic techniques.[10] Average polymer chain length, free-radical lifetime, quantum yield, etc. were determined in the course of this work. The effects of photopolymerization on the polymerized vesicle's surface morphology have been subsequently investigated with various molecular probes.[11,12] These results indicate that the net result of polymerization on vesicle surface morphology is to create a state of surface inhomogeneity in which bonded monomers are closer together than in the unpolymerized state and clefts are formed in the surface that exposed the hydrocarbon bilayer chains to water and solutes. Thus, in addition to stabilizing the vesicles, photopolymerization also markedly changes vesicle surface properties and morphology.

The vesicle photopolymerization simulation program was developed to obtain a graphical representation of the polymerization process and to provide a semiquantitative idea of the resulting vesicle surface inhomogeneity and polymer chain length distribution. The conceptual framework of the program is provided by the kinetic model presented in ref 10, and the parameter values proceed likewise from the experimentally obtained data.

The kinetics of the pulsed laser photopolymerization process were found to obey the proposed per vesicle governing equations

$$\frac{dM}{dt} = \gamma M \qquad \gamma = k_s - k_p \tag{1}$$

$$\frac{dM\cdot}{dt} = -\nu M\cdot \qquad \nu = k_m + k_s = \text{(effective free-radical lifetime)}^{-1} \tag{2}$$

$$M(0) = M_0 - M\cdot_0 = M_0(1 - \phi_r \epsilon E) \tag{3}$$

where $M(t)$ is the number of remaining unbonded monomers at time t, $M\cdot(t)$ is the number of free radicals, and the rate constants k_s, k_p, and k_m refer to the free-radical deactivation, polymerization step, and nonpolymer photoproduct forming step, respectively. The meaning of the "effective free radical lifetime" will be discussed below. ϵ refers to the polymerizable monomer's extinction coefficient (in cm^2/monomer) at the wavelength of the laser used, ϕ_r is the quantum efficiency of free-radical formation for photoexcited monomers, and E is the average energy/cm^2 in the sample cuvette per laser pulse. Figure 2 summarizes the proposed kinetic scheme for the vesicle photopolymerization. A full account of the considerations and approximations leading to eq 1-3 are given in ref 10.

The final time-dependent solution between laser pulses for eq 1 is

$$M(t) = M_0 - M\cdot_0 + \frac{\gamma M\cdot_0}{\nu}(1 - e^{-\nu\cdot t}) \tag{4}$$

The remaining monomer population after n laser pulses is given by

$$M(n) = M_0(1 - \eta)^n \tag{5}$$

where

$$\eta = \phi_r \epsilon E k_p/(k_m + k_s) \tag{6}$$

Using laser flash photolysis in conjuction with conventional absorption spectrophotometry allows the determination of ϕ_r, ν, k_p, and the average chain length according to

$$\text{average chain length} = \frac{k_p}{(k_m + k_s)} = \frac{\eta}{\phi_r \epsilon E} \tag{7}$$

The simulation program is not concerned with the time-dependent dynamics of the photopolymerization as

* Address correspondence to Physics Department, Tulane University, New Orleans, LA 70118.

0024-9297/85/2218-2402$01.50/0

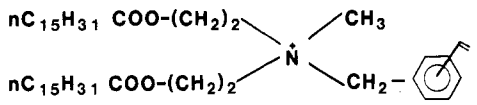

Figure 1. Polymerizable quaternary ammonium surfactant monomer used in the determination of the kinetic model of surfactant vesicle photopolymerization.

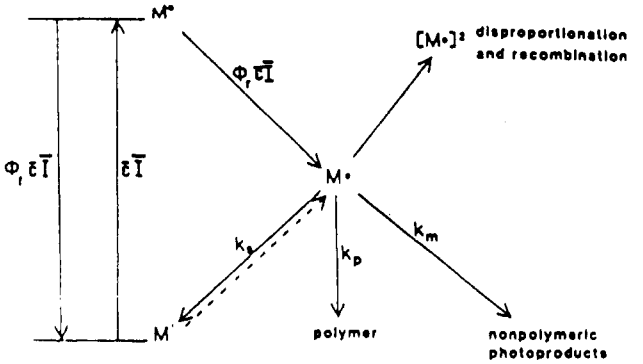

Figure 2. Proposed kinetic scheme for surfactant vesicle photopolymerization.

given in solution 4 but seeks, rather, to incorporate the results of these kinetics into a model for predicting changes in the polymerized surfactant vesicle morphology.

Simulation Procedure

Program SURPOL (surface polymerization) was developed by assuming an initial hexagonal packing of the surface monomers in the unpolymerized vesicles and assigning x and y coordinates to the monomers on a square patch of the vesicle surface. Hexagonal packing is the most efficient way to distribute objects of approximate cylindrical symmetry on a surface, especially when a high degree of organization and cooperativity is present, such as in surfactant vesicles below their phase-transition temperature. In addition to the coordinates, a flag is assigned to each monomer to monitor whether it has become a free radical or a link in a polymer chain or remains yet unpolymerized.

Program SURPOL works as follows: The person running the program specifies how large a sample patch of the vesicle is desired for the simulation and how many free radicals are to be generated during the simulation. Results for average intermonomer separation and other morphological quantities began to converge for total monomer fields greater than about 256, whereas the chain-length distribution results did not converge until at least about 1156 monomers were used (for initial average chain length of 15). The maximum monomer number in the sample available per run was 6400. The number of free radicals selected corresponds experimentally to the total irradiation of the vesicles and thus to the final degree of photopolymerization. The equilibrium separation between monomers in the unpolymerized vesicles is entered. The experimentally determined value for interheadgroup spacing determined in ref 10 is 10.0 Å. The polymer link length, as determined from ref 13 and extended to the monomers at hand, is also entered. The initial average number of links per polymer chain, as determined in ref 10, is entered along with the number of free radical/monomer encounters per free radical before the latter's deactivation. This quantity is proportional to the free-radical lifetime estimated in ref 10.

After these parameters are entered, the initial x and y coordinates for each monomer in the sample patch are assigned. The actual chain length for the free radical about to propagate is determined by making the entered average chain length the mean of a Gaussian distribution with standard deviation equal to the square root of the mean value and randomly choosing a chain length out of the distribution. Polymerization then begins by randomly choosing one of the monomers to become a propagating free radical. The flag for this monomer is set to the integer value "2" to indicate its free-radical status. The free radical then randomly chooses one of its six neighbors, thus simulating the diffusion-controlled free radical/monomer encounters that lead to polymer link formation. If the neighbor is yet unbonded, i.e., still has a "0" flag value, a link is formed and the monomer is pulled toward the free radical up to the specified polymer link distance along the line segment connecting the two. The coordinates of the monomer are then updated and its flag value set to "1" to indicate its status as a bonded monomer. If the randomly chosen monomeric neighbor of the free radical is already bonded in a polymer segment, a new neighbor is randomly chosen; i.e., the free radical continues its diffusion, and the same procedure as just described is applied to determine if a link is formed and the monomeric coordinates updated. If the free radical has no free neighbors, it is trapped or surrounded by bonded monomers and thus cannot propagate. Such a free radical is then deactivated. If the random search for an unbonded neighbor fails to turn up a suitable candidate after the number of tries dictated by the free radical/monomer encounters entered at the program's outset, the free radical is likewise deactivated.

It should be noted that the immediate bonding of a free radical to an unbonded monomer when the latter is found in the simulation is really a simplification of the polymerization process. The rotational anisotropy data from ref 10 indicate that the styrene groups diffuse about rotationally on the order of 1 ns and presumably make near encounters with their neighbors on this same time scale. The inverse of the polymerization rate constant, $1/k_p$, gives the average time of formation per link. Though not known to great accuracy, the time for link formation is on the order of 10^{-3} s.[10] This indicates that the styrene free radical is either relatively unreactive or needs a precise geometrical conjuncture with a neighbor before a polymer link is formed. The free radical may need on the order of a million near encounters with its bondable neighbors before forming a polymer link, and programming such a low success rate into the simulation would obviously slow the program down to an unacceptable pace. Since the program is not concerned with time-dependent kinetics, it was deemed unnecessary to include the probability for a successful link every time that a monomer/free radical encounter occurred. Likewise, it was not necessary to explicitly include lateral diffusion of monomers into the simulation. The presence of a monomer next to a free radical, whether the monomer was initially present upon free-radical formation or diffused there laterally, was the sole criterion for link formation. Thus, in program SURPOL, the finding of a bondable neighbor and linking to it by a free radical is understood to be preceded by a long series of unsuccessful diffusion-controlled free radical/bondable neighbor encounters.

The propagation of the polymer chain after making the first link continues in the manner described above: The newly bonded monomer becomes the propagating free radical (though its status remains as "1" so that only the initial free radical has status of "2") and randomly searches out and bonds to a free monomeric neighbor in the fashion just described. The chain continues to propagate either until the specific chain length chosen at the outset from the Gaussian distribution is reached, or until the free radical is trapped and can no longer propagate, or until

the free radical is deactivated by the prespecified lifetime limit. Another integer array is used to store the chain length for each free radical generated, in the order of generation.

During the course of the simulated polymerization process the growth of the polymer chain is graphically displayed on the computer terminal screen. When the number of chains reaches the initially specified limit, no more free radicals are generated, and the polymerization stops. The program proceeds to calculate the distance between all the monomers, both the bonded and remaining unbonded ones, in the sample patch and sorts these distances into intervals in a separation array. A plot of number of intermonomer separations vs. separation distance is then generated. The monomers that have gone into polymer chains now have a uniform separation which is smaller than the equilibrium separation. The unbonded monomers contribute to a peak at the initial unbonded separation. Other monomers have been distanced from each other by the contractions due to the polymer bond length. This effect manifests itself in a tail in the distribution lying above the unpolymerized equilibrium separation. It is this latter portion of the distribution that leads to the opening up of the vesicle surface and to the formation of clefts.

At this point in the program much information for further analysis is still available in the various arrays, and the program continues as follows: The percentage of monomers remaining intact (i.e., still with their double bonds) is calculated. The percentage of separations in the total array of separations (with $3(NM - 1)(NM - 1)$ elements, NM = number of monomers originally present) at greater than the equilibrium separation is calculated. This gives an idea of what percentage of the surface potentially contains clefts, i.e., areas of greater than equilibrium separation. The intermonomer distance for which 50% of the greater than equilibrium separations are larger is calculated next. This quantity gives a rough idea of the linear dimension of the median cleft. Since there is no reason to expect any type of geometrical symmetry or pattern for the clefts, this distance should not necessarily be construed as the "diameter" of a cleft, but rather as an approximation of the average linear dimension given by

$$\bar{l} = \frac{1}{\pi}\int_0^{\pi} l(\theta)\, d\theta \tag{8}$$

where $l(\theta)$ is the linear open area of the cleft as a function of polar angle θ in the plane of the vesicle surface.

The average intermonomer separation, excluding the population of separations at the polymer bond length, is also calculated for contrast with the previously calculated mean separation. The mean is calculated only for the separations at greater than the equilibrium intermonomer separation, whereas the average separation takes into account all intermonomer separations except the peak at the bond length.

In order to have a gauge of the degree of surface inhomogeneity that is caused by the photopolymerization, a surface inhomogeneity parameter is defined as

$$\text{inhomogeneity parameter} = \beta = \frac{2}{N(N-1)} \sum_{i=1}^{N} \frac{n_i(N - n_i)}{(1 + n_i)} \tag{9}$$

Here N refers to the total number of intermonomer separations, $N = 3(NM - 1)(NM - 1)$ (NM = number of monomers in the simulation) and n_i refers to the number of separations in the length interval i. The length intervals have a width equal to the value of the longest intermonomer separation in the array divided by the total number of separations, N. Though the definition of β in this way is arbitrary, it does have the following useful characteristics: If all the intermonomer separations are equal, $n_i = N\delta(ES - L_i)$ (ES is the equilibrium intermonomer separation, L_i is the length interval i, and δ is the discrete delta function), $\beta = 0$; i.e., the surface is completely homogeneous. If all the monomers are at a unique distance from each other ($n_i = 1$ for all i), $\beta = 1$, which corresponds to complete surface inhomogeneity. The notion of dividing the separation intervals into as many intervals as total separations arises as an analogy to the concept of state degeneracy in statistical physics. Instead of multiple occupation of, for example, an energy level, there can be multiple occupation of a separation interval in the above-defined inhomogeneity parameter. Complete surface homogeneity with $\beta = 0$ corresponds to complete separation degeneracy, where one separation interval is occupied by the entire population of separations.

The average chain length entered at the beginning of the program defines the mean of a distribution from which the chain lengths are drawn during the simulation. The particular chain length selected at random from the distribution for a given free radical, however, is just the suggested maximum length for that chain. This does not mean that the chain cannot terminate prematurely due to radical entrapment or by exceeding the radical lifetime in its search for bondable neighbors. Indeed, as the polymerization progresses, it should be expected that fewer and fewer chains reach their suggested maximum value because of the ever-decreasing number of available unbonded neighbors. These notions are made more concrete by taking advantage of the polymerization history contained in the various flag arrays. From these SURPOL constructs graphs, at the end of the simulation, of the number of chains vs. chain length, the weight-average chain length vs. chain length, and chain length vs. the logarithm of the photopolymerizing laser energy deposited.

Both sides of the vesicle were considered to polymerize independently of each other. This is because vesicles with polymerizable groups in the monomeric heads were being dealt with. The two polymerizing surfaces are thus separated by about 50 Å. The surface clefts formed are expected to be shallow, involving gauche turns or kinks only in the first few carbons of the hydrophobic chains. If disturbances in the surface packing due to polymerization were transmitted deep into the hydrocarbon interior, this would presumably disrupt the cooperativity of the bilayer structure and destabilize the vesicle. In fact, experimentally the opposite is observed; polymerized vesicles are stabler both over longer periods of time and with respect to more concentrated hostile environments (e.g., methanol) than unpolymerized vesicles. The alteration of surface morphology and formation of clefts is thus thought to proceed in the same fashion on both sides of the vesicle. The radii of the vesicles studied were experimentally determined to be 750 Å, so that the angle formed between the radial axes of two adjacent monomers, whose headgroups are separated by 10 Å, is only about 0.76°; i.e., the monomers are almost parallel, and radius of curvature considerations are negligible.

Results and Discussion

Program SURPOL allows simulation of vesicle photopolymerization not only according to the data obtained in ref 10 but also according to any change in polymerization parameters that might result as a change in the structure of the monomers used or of the polymerization process itself.

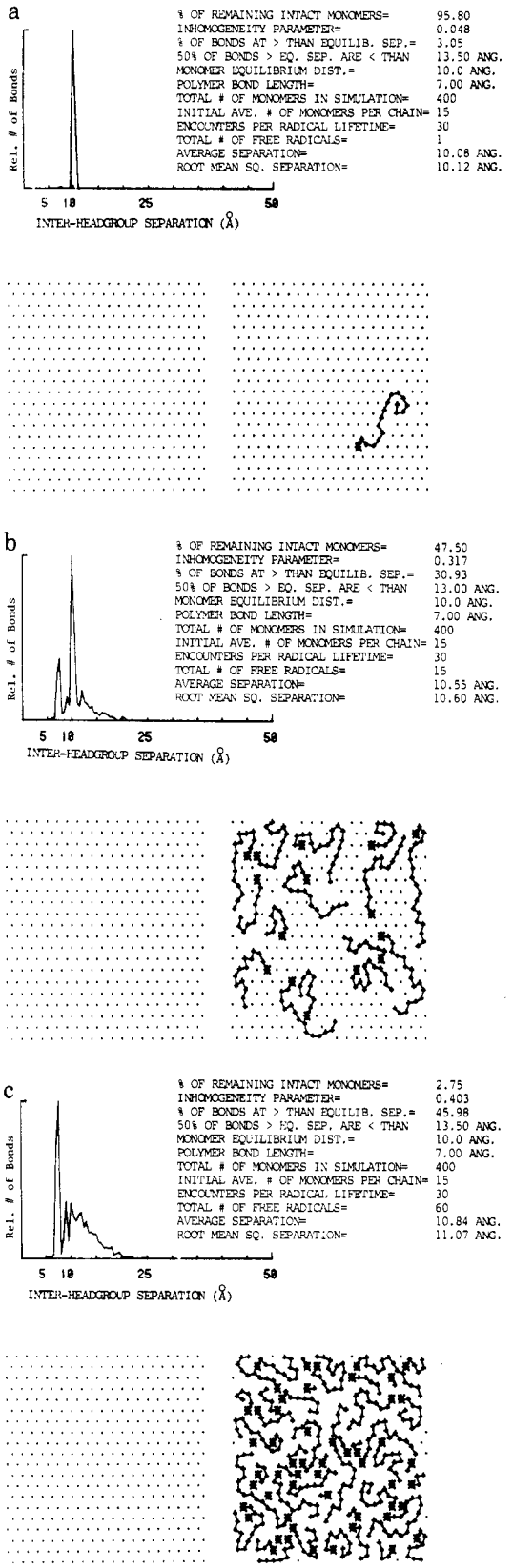

Figure 3. Postpolymerization intermonomer separation (left) and surface map (right) for (a) 4%, (b) 42%, and (c) 97% polymerization. The "average number of monomers per chain" refers to the initial average chain length discussed in the text.

The first series of simulations were carried out using the initial average value of 15 monomers per chain, a polymer bond length of 7 Å, 400 monomers in the sample patch, and an equilibrium separation of 10 Å. This series investigates the effect of increasing degree of polymerization on the parameters defined in the preceding section. Se-

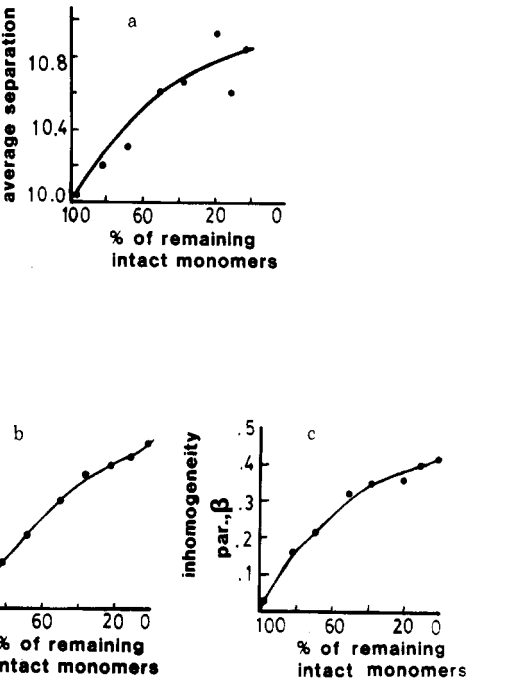

Figure 4. For the simulation carried to different final degrees of polymerization are plotted the percent of remaining (i.e., unlinked) intact monomers vs. (a) the average intermonomer separation, (b) the % of monomer separations that are greater than the prepolymerization intermonomer equilibrium separation, (c) the inhomogeneity parameter, β.

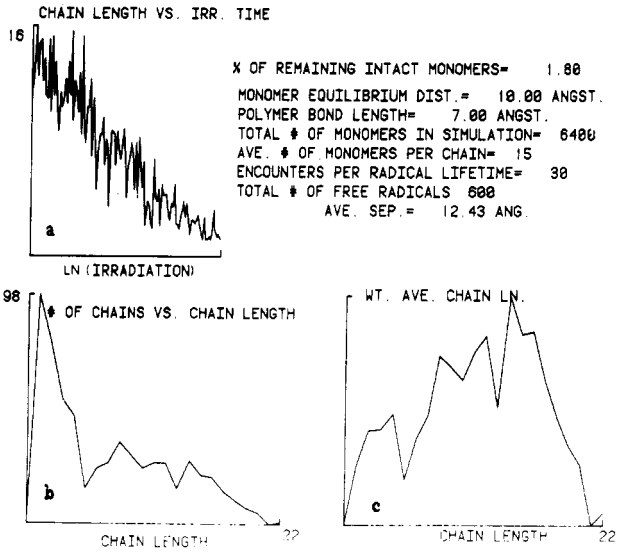

Figure 5. Chain length analysis portion of the simulation for the system of Figures 2, 3, and 4 carried out to over 98% final degree of polymerization: (a) decreasing chain lengths as a function of the natural logarithm of the irradiation (number of pulses for laser polymerization, time of irradiation for steady-state illumination). The decrease is due to increasing premature free-radical entrapment and deactivation as the photopolymerization progresses and leaves fewer available intact monomers. (b) number-average distribution of polymer chains. (c) weight-average distribution of polymer chains.

lected results of the stimulation for degrees of polymerization of about 3%, 48%, and 96% are shown in Figure 3a–c. At the right the polymer chains and remaining unbonded monomers are shown within the sample patch of the vesicle surface. On the left a plot of the number of intermonomer separations (with arbitrary normalization) vs. intermonomer separation (in angstroms) is given. Parts a–c of Figure 4 show plots of the average separation, the percentage of bonds of greater than the equilibrium sep-

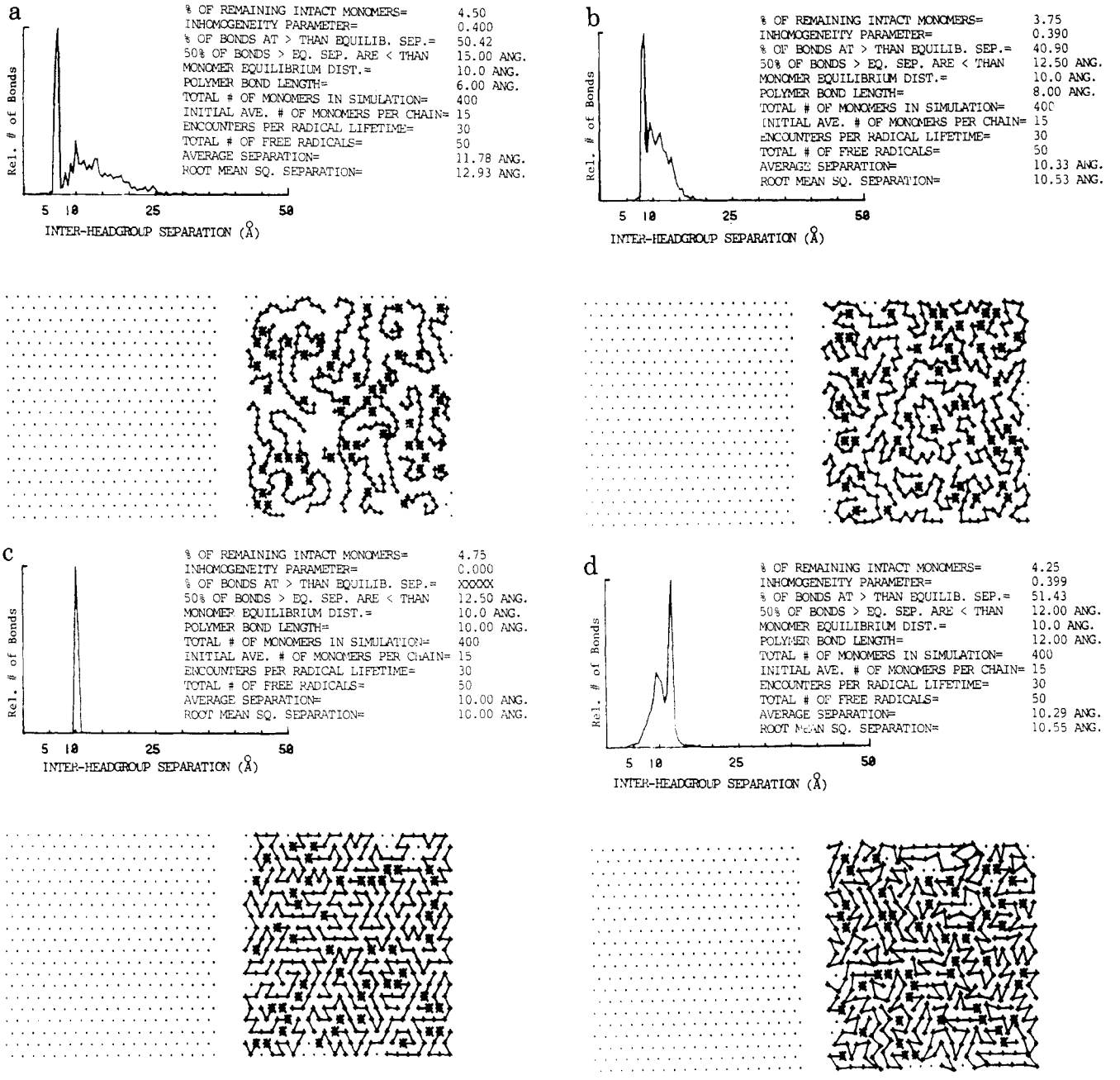

Figure 6. Simulation results for over 95% final degree of polymerization when the polymer bond length is varied, as could be achieved, e.g., by using different polymerizable monomers with different numbers of atoms between the headgroup and the polymerizable moiety. The bond lengths treated are (a) 6 Å, (b) 8 Å, (c) 10 Å, and (d) 12 Å.

aration, and β vs. the degree of polymerization.

As can be seen in Figure 3a–c, the mean interchain separation remains between 13 and 14 Å for any degree of polymerization. Thus the actual size of the surface clefts is not expected to change much as the degree of polymerization increases, rather openings which are roughly 30%–40% longer in their linear dimension than the equilibrium separation are expected to form as soon as polymerization begins. This suggests that partial polymerization may be a practical way of creating a specified number of cleft sizes of reasonably well-known dimension on the vesicle surface, so that a controlled number of guest molecules could be allowed to associate with the vesicle via the surface clefts. Since the polymerization kinetics have been well characterized,[10] it should be possible to produce any desired degree of polymerization to high accuracy according to the total amount of laser irradiation. The percentage of bonds at greater than the equilibrium separation, shown in Figure 4b, gives a way of correlating what percentage of the surface potentially contains clefts vs. the degree of polymerization.

It is possible, of course, that clefts in partially polymerized vesicles are "patched up" by free monomers driven by the entropy of mixing term in the chemical potential. For highly or completely polymerized vesicles, however, there are not enough free monomers around to "patch up" the clefts, so that regions of increased mean free area remain as a statistical certainty.

The average intermonomer separation is seen to rise weakly during the polymerization process to a maximum value only about 6%–9% greater than the equilibrium separation. This indicates that although there is a net statistical opening up of the vesicle surface with increasing polymerization, there is also a corresponding tendency of a fraction of the interchain monomers to approach each other more closely than in the equilibrium situation.

The inhomogeneity parameter, β, is seen to increase rapidly in the early stages of polymerization and then

begins to reach a plateau when the polymerization is over 50% complete. This means that in the early stages of polymerization the monomer separations rapidly begin to fill up previously unoccupied separation intervals, whereas in the latter stages the tendency of a fraction of the chains to approach each other more closely than the equilibrium distance, as well as the inherent limiting packing constraints, causes a degeneracy of occupation of the same separation intervals. This tendency can also be seen by regarding the behavior of the separation distributions in Figure 3, parts b and c. In these the tail of the distribution is seen to have fanned rapidly out toward higher separation values by the half-way polymerization stage and then begins to grow vertically and fill in during the latter stages. This filling in of the tail distribution causes less increase in β than the expansion of the tail toward higher unoccupied separation values, and so β begins to level out at a value of about 0.4.

Parts a–c of Figure 5 show the chain length analysis portion of program SURPOL for the case of full polymerization (>98%) in the first series of simulations. Figure 5a shows a plot of chain length vs. the logarithm of irradiation. Because of the process of free-radical trapping and decreasing number of available bondable neighbors the chain length decreases in time. The result is that there are many short chains in the final distribution (Figure 5b), although the final weight-average distribution of chain lengths (Figure 5c) is peaked near the initial average number of monomers per chain with which the program starts. The overall effect of the chain shortening vs. irradiation time is to perturb the weight-average chain-length distribution from a normal distribution to an asymmetric one in which there is a greater weighting and buildup on the short chain side. Recent direct determinations of polymer chain lengths have been made by using high-pressure liquid chromatography and substantiate the distributions calculated by SURPOL.[14]

Thus, the initial average chain length with which the program starts is not the overall average chain length, but rather the average chain length that would be obtained if free-radical trapping and deactivation did not whittle down the succeeding chain lengths as polymerization progresses. The initial average chain length is measured experimentally according to eq 7 during the early stages of the photopolymerization. The "effective free-radical lifetime" mentioned in eq 2 is the lifetime over which the free radical can continue to link to monomers. The effective lifetime ends when either there are no more bondable neighbors around the free radical or packing/geometrical constraints prohibit further bonding, even though the radical itself may continue to live considerably longer before being deactivated.

The actual physical origin of the maximum average chain length, however, while certainly residing in packing and topographical constraints, would be a very difficult parameter to model on theoretical grounds. Such a model would necessarily involve a complex statistical mechanical formulation to account for changes in hydrocarbon chain conformational structure, excluded-volume effects, steric effects, etc. This is beyond the scope and aim of the current simulation.

The next series of simulations was run by varying the polymer bond length and running the polymerization toward completion (<5% remaining monomers). Parts a–d of Figure 6 show the results of these simulations for equilibrium monomer separations of 10 Å and chain lengths of 6, 8, 10 and 12 Å, respectively. These would correspond to synthesizing different monomers containing

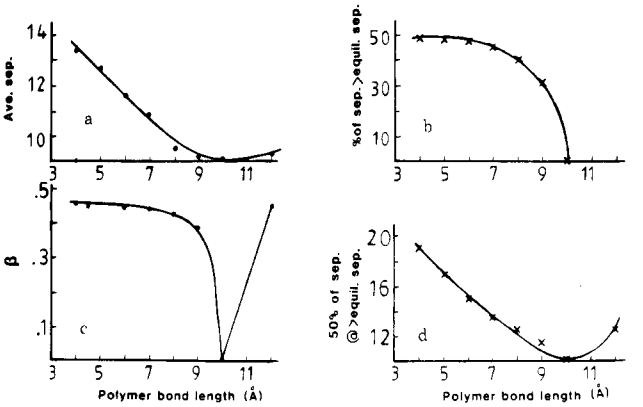

Figure 7. Plots of model parameters vs. polymer bond length on the vesicle surface: (a) average intermonomer separation; (b) percent of intermonomer separations that are greater than the prepolymerized intermonomer equilibrium distances; (c) inhomogeneity parameter, β; (d) median cleft size (in Å).

headgroups with such polymerizable groups as styrene with additional groups, such as methyls or esters, between themselves and the headgroup's nitrogen atom (to increase polymer bond length) or simple vinyllic groups (to decrease polymer bond length). Though the same average number of monomers per polymer chain was used as in the previous simulation (15), it is probable that one of the main factors determining chain length is the polymer bond length and resulting surface packing limitations. Thus, polymerizing monomers that result in shorter bond lengths might well shorten the chains, whereas longer bond lengths might lead to much more extensive chains. This assertion, however, is not provable by mere modeling and would require the synthesis of such monomers and a detailed determination of the polymerization kinetics and average chain length according to the methodology established in ref 10. The behavior of the model parameters is plotted in Figure 7a–d.

The inhomogeneity parameter increases sharply with polymer bond length as this latter moves away from the equilibrium separation by up to about 2 Å but then quickly reaches a plateau value of about 0.43 (Figure 7c). The same type of behavior is closely followed by the percentage of interchain bonds at greater than the equilibrium separation which reaches a plateau at about 50% (Figure 7b). At this point roughly half the surface potentially contains clefts. The average separation (Figure 7a) and mean-interchain separation (Figure 7d) both increase markedly as the bond length progressively differs from the equilibrium separation. The median cleft size increases faster than the difference between polymer bond length and equilibrium monomer separation. Thus, shortening the polymer chain length might result in significantly larger clefts. In contrast, matching the polymer bond length to the equilibrium separation might lead to no clefts, more extensive chains, and greater overall vesicle stability.

The last series of simulations was carried out by varying the average chain length and running the polymerization toward completion. The bond length was chosen to be 6 Å and the equilibrium separation to be 10 Å. Parts a–d of Figure 8 show the results of this series of simulations for average chain lengths of 2, 4, 7, and 10 monomers. The salient features are that cleft formation begins even for mere dimerization of the monomers, although the mean interchain separation, and hence cleft size, increases steadily for chains from two to four monomers long but then stays fairly constant for longer chain lengths. This must again be traceable to the limiting packing constraints on the surface, and so cleft size is only weakly related to polymer chain length. The monomer separation graphs

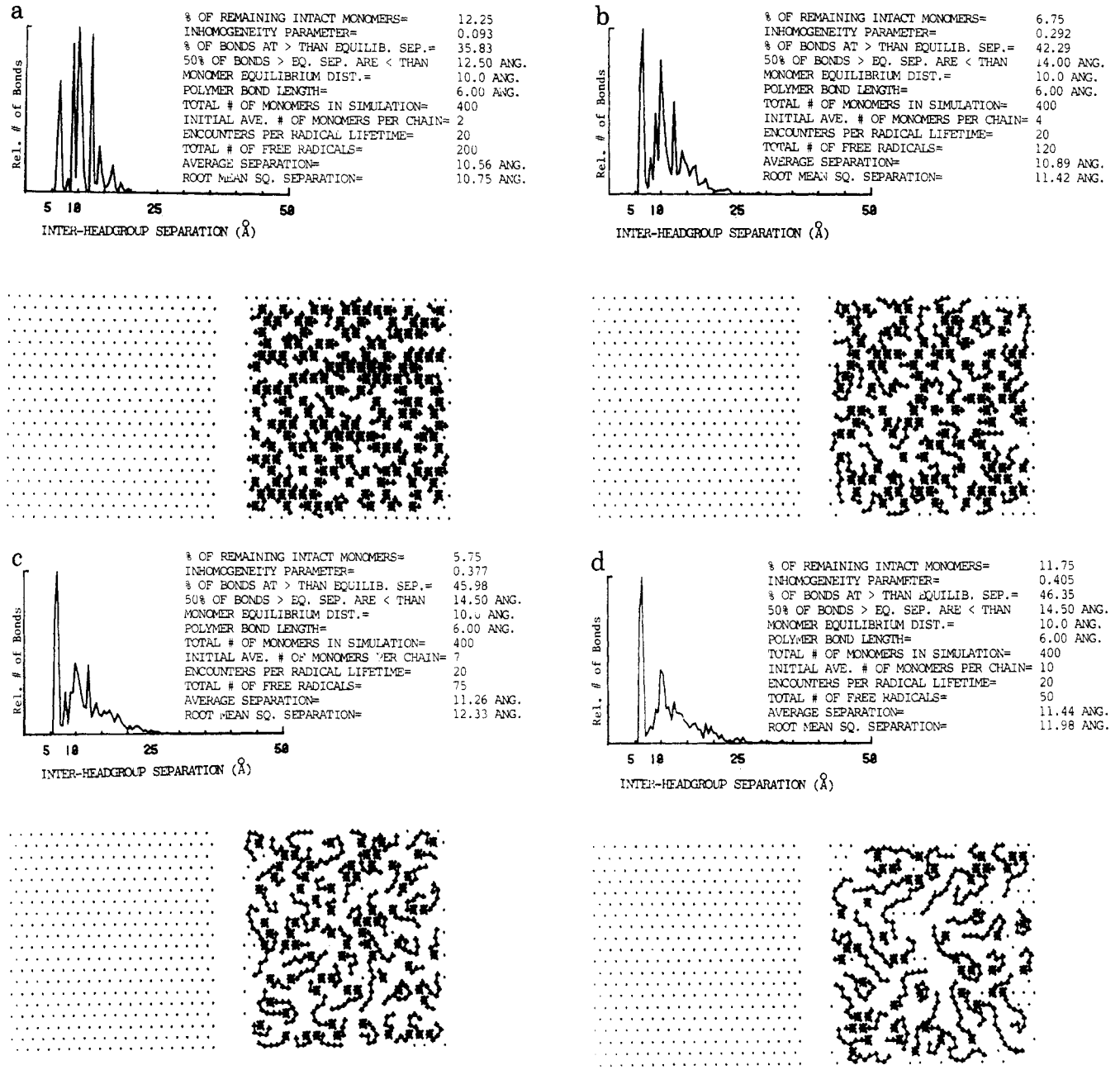

Figure 8. Simulation results for near complete polymerization for chain lengths containing (a) 2, (b) 4, (c) 7, and (d) 10 monomers.

in Figure 8a–d show that spikes appear for the cases of short chain length. This is also reflected in the low inhomogeneity parameters for these cases. Above about five monomers the distribution becomes less peaked, and the inhomogeneity parameter rises to its plateau value of about 0.41.

The three series of polymerization simulations described above have thus provided some new insights into the detailed changes in the surface morphology and inhomogeneity of the polymerized vesicles. SURPOL remains a flexible program that can be modified and refined to study more precisely the polymerization kinetics, packing restrictions, and results of functionalizing the polymerizable group onto other portions of the monomer (e.g., in the tail). Furthermore, the general approach applied to surfactant vesicles should be readily amendable to the simulation and analysis of surface effects and polymer distributions for other two-dimension polymerizable systems such as coatings and thin films.

A final point should be made concerning the oftenmentioned "clefts". These clefts are hypothetical and are identified with the areas of increased mean free area and intermonomer separation on the vesicle's surface which SURPOL graphically depicts and statistically analyzes. Experimental evidence that these clefts might actually exist comes from the increased association of molecular probes in polymerized vesicles in a more hydrocarbon environment vis-a-vis the unpolymerized case.[11,12] A physicochemical model might also predict the depth distribution of the clefts, in addition to the maximum chain length due to the surface packing constraints. Presumably the clefts are shallow, only reaching down a few carbons, so that the deep, cooperative bilayer structure is not upset: photopolymerization stabilizes these vesicles, it does not disrupt them.

Acknowledgment. Support from the National Science Foundation and Eastman Kodak is gratefully acknowledged.

Registry No. $[n\text{-}C_{15}H_{31}CO_2(CH_2)_2]_2N^+[CH_3][CH_2C_6H_4CH{=}CH_2]Cl^-$, 88703-85-9; $[n\text{-}C_{15}H_{31}CO_2(CH_2)_2]_2N^+[CH_3]$-

$[CH_2C_6H_4CH{=}CH_2]Cl^-$ (homopolymer), 98065-26-0.

References and Notes

(1) Martonosi, A. "Membranes and Transport"; Plenum Press: New York, 1982.
(2) Papakadjopoulos, D. *Ann. N. Y. Acad. Sci.* **1978**, *308*, 1–468.
(3) Fendler, J. H. "Membrane Mimetic Chemistry"; Wiley Interscience: New York, 1982.
(4) Kunitake, T.; Okakata, Y.; Shimomura, M.; Yusanami, S.; Takarase, K. *J. Am. Chem. Soc.* **1981**, *103*, 5401–5412.
(5) Barraud, A.; Rosillo, C.; Ruaudel-Teixler, A. *J. Colloid Interface Sci.* **1977**, *62*, 509–563.
(6) Bader, H.; Ringsdorf, H. *J. Polym. Sci., Polym. Chem. Ed.* **1982**, *20*, 1623–1628.
(7) Day, D.; Ringsdorf, H. *Makromol. Chem.* **1978**, *180*, 1059–1063.
(8) Regen, S. L.; Singh, A.; Oehme, G.; Singh, M. *J. Am. Chem. Soc.* **1982**, *104*, 791–794.
(9) O'Brien, D. F.; Whitesides, T. H.; Klingbiel, R. T. *J. Polym. Sci., Polym. Lett. Ed.* **1981**, *19*, 95–101.
(10) Reed, W.; Guterman, L.; Tundo, P.; Fendler, J. H. *J. Am. Chem. Soc.* **1984**, *106*, 1897–1907.
(11) Reed, W.; Hauser, H.; Lasic, D.; Fendler, J. H. *Macromolecules*, in press.
(12) Nome, F.; Reed, W.; Politi, M.; Tundo, P.; Fendler, J. *J. Am. Chem. Soc.* **1984**, *106*, 8086–8093.
(13) David, C.; Baeyens-Volant, D. *Ann. N. Y. Acad. Sci.* **1981**, *366*, 341–355.
(14) Serrano, J.; Mucino, S.; Millan, S.; Reynoso, R.; Fucugauchi, L.; Reed, W.; Nome, F.; Tundo, P.; Fendler, J. H. *Macromolecules*, in press.

Ethylene Terpolymerization with 1-Butene and Long-Chain α-Olefins: Reactivity Ratios

J. V. Seppälä

Neste Oy Research Centre, 06850 Kulloo, Finland.

Received May 10, 1985

ABSTRACT: The terpolymerization equation has been applied to ethylene terpolymerization with 1-butene and C_{10}, C_{12}, and C_{16} α-olefins. The six binary reactivity ratios in the terpolymerization equation were determined by a computer search for each terpolymerization. The calculated polymer compositions were compared with the compositions determined by ^{13}C NMR spectroscopy, and the results generally agreed within 1 wt %. The terpolymerization behavior could be explained with the determined reactivity ratios and the terpolymerization equation.

Introduction

The copolymerization of ethylene with linear α-olefins has recently found wide industrial applications in the synthesis of branched polyethylenes under low pressure using Ziegler–Natta catalysts.

In the calculation of Ziegler–Natta-type polymerizations, copolymerization equations have been successfully applied.[1,2] In a two-component copolymerization, several methods have been developed for the determination of the reactivity ratios.[1,3–10] In the case of terpolymerization, the situation is more complicated so computer-searching algorithms have been applied.[11–13]

In the binary copolymerizations of ethylene with different α-olefins, the reactivity ratios have been studied rather extensively.[14–22] For terpolymerizations of ethylene with 1-butene and long (C_{10}–C_{16}) α-olefins, a synergistic effect has been reported in the reactivities of 1-butene and the long-chain α-olefins,[23–25] though reactivity ratios for this case had not been determined earlier.

Experimental Section

In slurry-type coordination polymerizations, the reaction medium was *n*-heptane. $TiCl_3 \cdot {}^1/_3AlCl_3$ was used as the catalyst and Et_3Al as cocatalyst. 1-Butene, 1-decene, 1-dodecene, and 1-hexadecene were employed as comonomers with ethylene. The polymerization temperature was 90 °C and the hydrogen partial pressure 300 kPa. The steady-state conditions were approximated by keeping the comonomer conversions always less than 15% and by adding ethylene in a semibatch way. The polymerization procedures and the analytical methods have been reported elsewhere.[23–25]

It has shown previously that monomer concentrations in polymerizations have a synergistic effect on the comonomers and, thus, the composition of the polymer product. The reactivity of the long α-olefins in the presence of 1-butene has been considerably higher than could be assumed based on binary ethylene–α-olefin copolymerizations.[23–25] The effect of 1-butene addition on ethylene copolymerization with 1-dodecene can be seen clearly in Figure 1.

It is often assumed that terpolymerization can be calculated with the simple terpolymerization equation using reactivity ratios determined with binary copolymerizations.[26–30] That assumption is unnecessary when the six reactivity ratios in the terpolymerization equation are searched by a computer algorithm. In this algorithm, the binary reactivity ratios (r_{ij}) are adjusted to give the most suitable compositions calculated with the terpolymerization equations. The sum of the squares of the deviations can be used as the function to be minimized.

The SIMPLEX algorithm was applied for estimation of parameters of nonlinear models. It was originally developed by Nelder and Mead,[31] though the version used in this study has been published by Fredenslund et al.[32]

A simple terpolymerization equation developed by Alfrey and Goldfinger[26] was used in the form

$$dc_1/dc_3 = \{c_1(c_1r_{23}r_{32} + c_2r_{31}r_{23} + c_3r_{32}r_{21}) \times (c_1r_{12}r_{13} + c_2r_{13} + c_3r_{12})\}/\{c_3(c_1r_{12}r_{23} + c_2r_{13}r_{21} + c_3r_{12}r_{21})(c_3r_{31}r_{32} + c_1r_{32} + c_2r_{31})\} \quad (1)$$

$$dc_2/dc_3 = \{c_2(c_1r_{32}r_{13} + c_2r_{13}r_{31} + c_3r_{12}r_{31}) \times (c_2r_{21}r_{23} + c_1r_{23} + c_3r_{21})\}/\{c_3(c_1r_{12}r_{23} + c_2r_{13}r_{21} + c_3r_{12}r_{21})(c_3r_{31}r_{32} + c_1r_{32} + c_2r_{31})\} \quad (2)$$

where c_i is the molar concentration of monomer i (i = 1, 2, 3) and r_{ij} ($i \neq j$) is the appropriate binary reactivity ratio. In the present case subscripts 1, 2, and 3 refer to ethylene, 1-butene, and the long-chain α-olefin, respectively. The compositions of terpolymers prepared in sta-

0024-9297/85/2218-2409$01.50/0